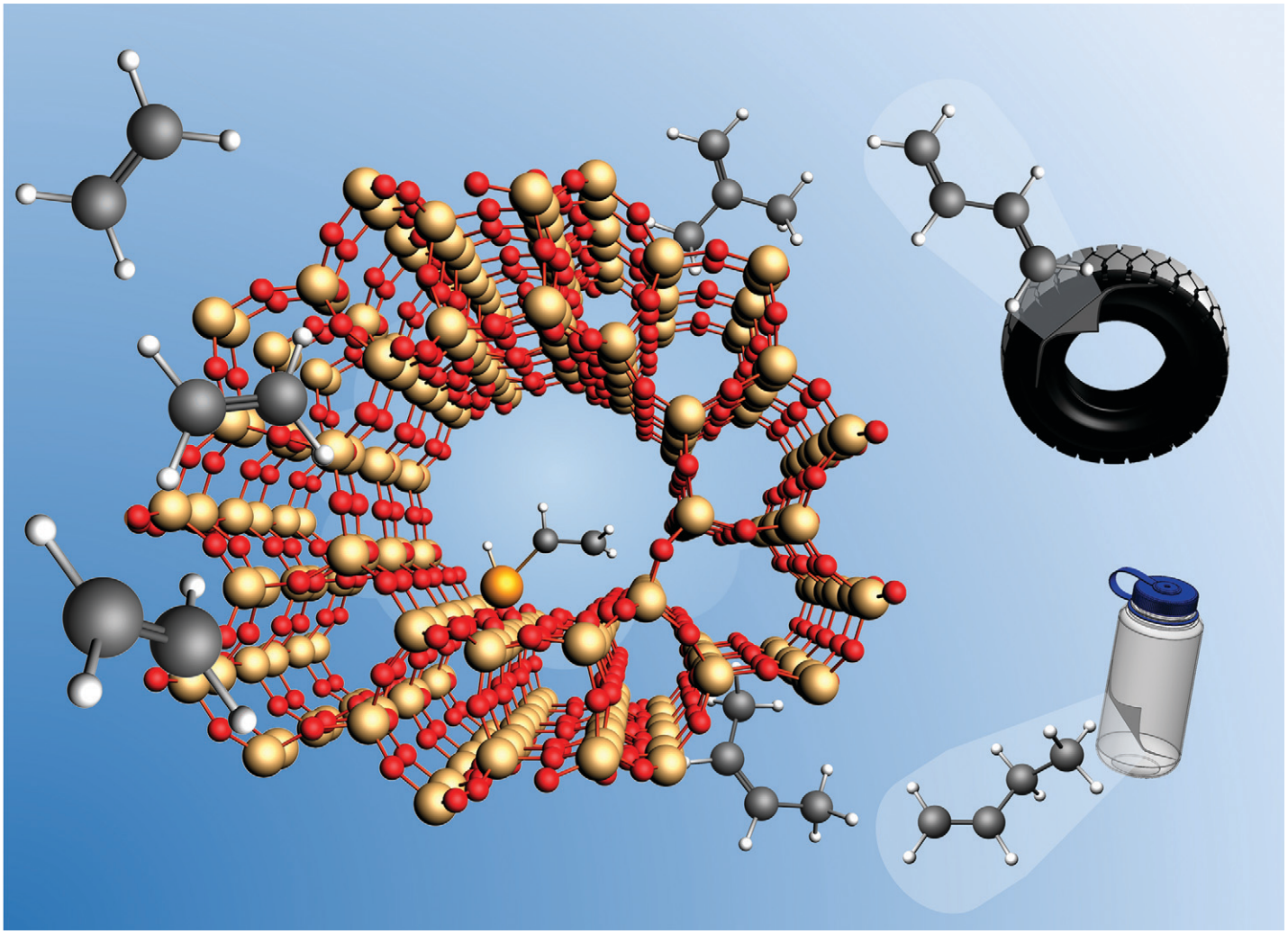

Showcasing research from Pacific Northwest National Laboratory.

Catalytic activation of ethylene C–H bonds on uniform d^8 Ir(I) and Ni(II) cations in zeolites: toward molecular level understanding of ethylene polymerization on heterogeneous catalysts

Ethylene polymerization is a large-scale catalytic process employed in the manufacture of an abundance of consumer products. In this work, uniform d^8 metal centers are synthesized and exploited to reveal the long-debated intermediates of ethylene polymerization whereby the oxidative addition of ethylene generates d^6 metal vinyl hydride complexes. The dehydrogenative coupling of ethylene leads to the formation of butenes and butadiene under mild conditions on the zeolite-supported Ir(I) and Ni(II) catalysts. The findings provide new molecular-level understanding to an important chemical process.

As featured in:

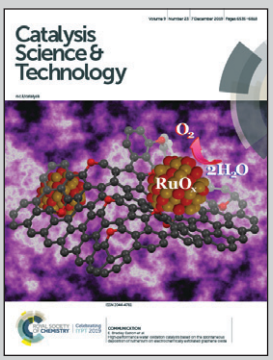

See Nicholas R. Jaegers, Konstantin Khivantsev, János Szanyi *et al.*, *Catal. Sci. Technol.*, 2019, **9**, 6570.

ROYAL SOCIETY OF CHEMISTRY | Celebrating IYPT 2019

rsc.li/catalysis

Registered charity number: 207890

Catalysis Science & Technology

PAPER

View Article Online
View Journal | View Issue

Cite this: *Catal. Sci. Technol.*, 2019, **9**, 6570

Catalytic activation of ethylene C–H bonds on uniform d^8 Ir(I) and Ni(II) cations in zeolites: toward molecular level understanding of ethylene polymerization on heterogeneous catalysts†

Nicholas R. Jaegers, ‡*ab Konstantin Khivantsev, ‡*a Libor Kovarik, a Daniel W. Klas,a Jian Zhi Hu, a Yong Wang ab and János Szanyi ‡*a

Received 20th July 2019,
Accepted 16th October 2019

DOI: 10.1039/c9cy01442j

rsc.li/catalysis

The homolytic activation of the strong C–H bonds in ethylene is demonstrated, for the first time, on d^8 Ir(I) and Ni(II) single atoms in the cationic positions of zeolites H-FAU and H-BEA under ambient conditions. The oxidative addition of C_2H_4 to the metal center occurs with the formation of a d^6 metal vinyl hydride, explaining the initiation of the olefin-polymerization cycle on d^8 M(I/II) sites in the absence of pre-existing M–H bonds. Under mild reaction conditions (80–220 °C, 1 bar), the catalytic dimerization to butenes and dehydrogenative coupling of ethylene to butadiene occurs over these catalysts. 1-Butene is not converted to butadiene under the reaction conditions applied. Post-reaction characterization of the two materials reveals that the active metal cations remain site-isolated whereas deactivation occurs due to the formation of carbonaceous deposits on the zeolites. Our findings have significant implications for the molecular level understanding of ethylene conversion and the development of new ways to functionalize C–H bonds under mild conditions.

Zeolite-supported transition metals (single atoms, clusters, nanoparticles, *etc.*) represent an important class of materials with uses in chemical industry, emissions control, and as model systems to derive structure–function properties in catalysis.[1–9] Among them, d^8 metals such as Ni(II), Rh(I), Ir(I), Pt(II), and Pd(II) have been the focus of many studies to better understand the genesis, speciation, and stability of such species for reactions such as hydrogenations, oxidations, as well as ethylene transformation (di- and oligomerization to butenes and higher oligomers).[10–13] For example, it was shown first in the 1950s that Rh(I)$(CO)_2$ and Ir(I)$(CO)_2$ species can be stabilized on oxide supports[14,15] and are active for ethylene conversion to butenes at room temperature, retaining their site-isolated nature after catalysis.[16–18]

The Rh ligand environment is tunable and hydrogen promotes butene formation despite not directly participating in the dimerization reaction (*i.e.*, $2C_2H_4 \rightarrow C_4H_8$).[12,17,18] This effect was explained in some studies by H_2 enhancing butene desorption on $(Rh(C_2H_4)_2/HY)$.[16] Recently, however, the hydrogen partial pressure dependence of ethylene dimerization was systematically measured on $Rh(CO)_2$, $Rh(CO)(C_2H_4)$, $Rh(CO)(H)$,[17] and $Rh(NO)_2$[12] complexes supported on HY zeolites. Positive reaction orders of ~0.7–1 confirmed that hydrogen indeed promotes dimerization, where H_2 was shown to improve the rate of ethylene dimerization up to ~10 fold.[12,17] This was attributed to the formation of metal-hydride-supported species (observed and characterized experimentally[12,17,18]) which provide a low-energy pathway for dimerization *via* facile insertion of pi-coordinated ethylene into the M–H bond to form an M-ethyl moiety which subsequently migrates into another pi-coordinated ethylene to form a Rh-butyl species prior to facile β-H abstraction to produce butene-1.[12] This attribution was subsequently supported for ethylene dimerization on Ni/BEA, although Ni–H species were not observed directly.[19] Until now, it remained unclear how ethylene, in the absence of M-hydride species, can polymerize considering the importance of M–H intermediates in the Cossee–Arlman mechanism. Theoretical studies have identified potential mechanisms for ethylene dimerization on Ni/BEA where the metallocycle, proton-transfer, and Cossee–Arlman mechanisms were compared.[20] Also considered was the non-catalytic formation of a nickel vinyl intermediate *via* the heterolytic activation of a C–H bond over Ni(II)–O bond followed by the formation of an active Ni center.[20]

[a] *Institute for Integrated Catalysis, Pacific Northwest National Laboratory, Richland, WA 99352, USA. E-mail: Nicholas.Jaegers@pnnl.gov, Konstantin.Khivantsev@pnnl.gov, Janos.Szanyi@pnnl.gov*
[b] *Voiland School of Chemical Engineering and Bioengineering, Washington State University, Pullman, WA 99163, USA*

† Electronic supplementary information (ESI) available. See DOI: 10.1039/c9cy01442j

‡ These authors contributed equally.

In this study, we demonstrate: 1). preparation and characterization of highly uniform d^8 metal species. Ni(II) was selected because it has been a challenge to prepare well-defined uniform Ni-zeolite species. We have previously prepared d^8 Pt(II) and Pd(II) species[9] in zeolite uniformly and thus transferred this approach to a Ni/BEA system in order to unravel detailed structure catalytic–property relationships for the historically important system for ethylene polymerization. We also employ the well-defined square planar d^8 Ir(I)$(CO)_2$ complex anchored in zeolite FAU (like Ni(II)/FAU) because it grafts uniformly in zeolite and also has CO groups which, due to their high molar extinction coefficients and well-resolved nature, allow us to observe ligand changes with enhanced resolution. 2). We obtain the reactivity for ethylene couplings on those materials, showing similar trends for both d^8 metals 3). We resolve a longstanding uncertainty in heterogeneous ethylene polymerization, one of the largest catalytic processes. Though supported metal ions (d^8 such as Ni(II), Ir(I), Pd(II) or d^4 Cr(II)) perform this reaction without the initiator/co-catalyst, the mechanism for ethylene polymerization initiation and the relevant intermediates involved have remained elusive for the last 50 years. We resolve these uncertainties using state-of-the-art infrared studies supported by microscopy and solid-state NMR measurements[21] for d^8 metal cations on solid supports. In short, ethylene polymerization starts with the homolytic activation of the C–H bonds of ethylene on extremely electrophilic d^8 M sites, resulting in the formation of d^6 metal vinyl hydride complexes which further react with ethylene to form a vinyl ethyl d^6 metal fragment. From this fragment, 1-butene can form either *via* direct reductive elimination or a Cossee–Arlman type step involving alkyl chain growth through alkyl migration and insertion into M-ethylene bonds.

Though reported for other d^8 metals, it is not straightforward to generate uniform Ni(II) species since they may graft to both silanol nests and various extra-framework zeolite positions, evidenced by IR spectroscopy of CO adsorption.[19] This brought into question the true active center for ethylene oligomerization activity.[22] To better understand the active centers for ethylene dimerization, well-defined supported complexes of Ir(I) and Ni(II) were generated, characterized, and tested in this study. These active centers not only demonstrate activity to butenes, but butadiene as well; a notable result since 1,3-butadiene is a high-value commodity chemical (~10 million tons per annum) that serves as a precursor to a wide range of plastics and polymers. These reactions proceed *via* activation of C–H bonds of ethylene on a super electrophilic cationic metal center recently observed for a metal/zeolite system.[23]

A modified IWI method was previously used to produce atomically dispersed Pt and Pd in SSZ-13.[9] We slightly altered this procedure to synthesize 0.4 wt% Ni on BEA by reacting aqueous nickel nitrate with excess ammonia to produce a mononuclear Ni hexamine complex. This mitigates the formation of hydroxo-bridged Ni complexes, which are precursors to NiO nanoparticles, similar to the aqueous solution of $Pd(NO_3)_2$ that has the propensity to darken and form …–OH–Pd–OH–Pd–OH–… networks over time, even in acidic solutions.[9,24,25] The micropores of BEA zeolite (Si/Al ~ 12.5) were impregnated with this complex, dried in ambient air, and calcined at 550 °C in static air. Infrared spectroscopy of adsorbed CO on this material substantiates the exclusive formation of 1 type of Ni(II)–CO in BEA zeolite. The C–O stretching vibrational band of this species is located at 2211 cm^{-1} (Fig. 1A).

No NiO clusters or nanoparticles could be observed in the channels of BEA. EDS mapping confirmed the presence of Ni associated with BEA, corroborating the presence of uniform, isolated Ni sites in the sample (Fig. 1B and C and S1–S3†). Comprehensive interconversion maps of Ni(II)–CO, Ni(II)–NO, Ni(II)–C_2H_4, and Ni(II)(NO)(CO) complexes, never prepared through classical organometallic routes are discussed and available in the ESI† (Fig. S4–S17). These provide new insight into the Ni/Zeolite chemistry complementary to the previous pioneering studies of Petkov *et al.*[26] In particular, a new phenomenon in solid supported systems is identified whereby low-temperature CO adsorption produces 2 peaks at 2214 and 2204 cm^{-1} (Fig. S11†), that do not belong to the Ni(II)$(CO)_2$ dicarbonyl complex (evidenced by their contrasting interactions with C_2H_4 and stability under vacuum, Fig. S12 and S13†). However, CO adsorption at room temperature produces only 1 band at 2211 cm^{-1}. This indicates that at low temperatures, distinctive Al T-sites exist while at room temperature these sites become degenerate, possibly due to the flexibility of the zeolite framework or relativistic effects,

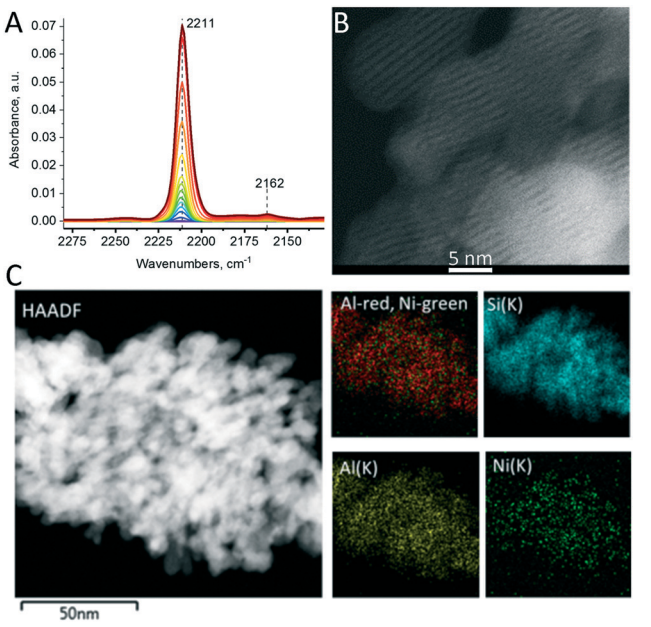

Fig. 1 A). FTIR during CO adsorption on dry 0.4% Ni/BEA, P(CO)max = 5 Torr (the band at 2162 cm^{-1} represents adsorbed ^{13}CO molecules) B). High-resolution HAADF-STEM image of the 0.4% Ni/BEA material: straight channels in BEA nanocrystals are clearly imaged. No NiO clusters or particles observed (additional HAADF-STEM images provided in Fig. S2†) C). EDS mapping of Ni, Al, Si, and Ni/Al overlay in 0.4% Ni/BEA.

revealing only the 2211 cm^{-1} feature from CO adsorption on super electrophilic Ni(II)/2Al centers.

Unlike Rh(I)/FAU complexes, for which initial ligand environment impacts ethylene dimerization,[12,17,18] both Ni(II)–CO and Ni(II)–NO undergo ligand replacement by ethylene to form Ni(II)–C_2H_4 complex under ambient conditions and lower temperatures (Fig. S5, S9 and S13–S15†). This material was active for ethylene transformation to butenes, demonstrating that Ni(II) in the ion-exchange position is active for catalysis (Table S1†). Remarkably, 80 °C was sufficient to observe activity for both butadiene as well as butenes (1-butene as well as *cis*- and *trans*-2-butene) formation. Selectivity initially favored butadiene at 120 °C (~65%, TOF ~122 h^{-1} with respect to butadiene formed and ~240 h^{-1} with respect to ethylene molecules reacted, Table S1†), however, selectivity quickly dropped to ~10% within the first 30 minutes (TOF ~ 10 h^{-1}). Above 180 °C, activity for butadiene production is enhanced with selectivity around 20–30% on a molar basis at 200 °C and initial TOF ~200 h^{-1}. Even at elevated temperatures, deactivation is observed both for butene and butadiene production with time on stream (Fig. S18†).

These results are noteworthy since C–H bond activation in ethylene (22 kJ mol^{-1} stronger than methane at 298 K) is a challenging catalytic step. Accordingly, functionalization of ethylene typically involves reactions with its C=C bond and not the C–H bond directly. By activating the C–H bond in ethylene, the formal coupling of two vinyl C_2H_3 fragments enables the formation of butadiene.

Catalytically, butadiene can be produced by dehydrogenation of *n*-butane and 1-butene (Houdry process) or by ethanol conversion to butadiene, hydrogen, and water over a mixed metal oxide catalyst (Lebedev and Ostromyslenski process). These catalytic processes with unpromoted catalysts produce butadiene unselectively and are energy intensive (400–700 °C).[27] The best current processes based on ethanol show excellent selectivity to butadiene for promoted materials (>90%) whereas the unpromoted, historically important Ta-containing material has a selectivity of ~15%. However, this process relies on a low ethanol feed rate (GHSV), features turnovers of ~1 h^{-1} at 320 °C, and suffers deactivation due to formation of polymeric carbonaceous deposits.[28,29]

Though pathways from alcohol feedstocks exist, the catalytic conversion of ethylene to butadiene remains effectively unprecedented with just a few examples proposed. In 1983, $(C_5(CH_3)_5)_2Ti(C_2H_4)$ complexes in aromatic solvents were suggested to convert ethylene into 1,3-butadiene and ethane at 25 °C and ~4 atm in a sealed batch reactor, though the reported TOF after one year was ~1–2 $year^{-1}$, rendering catalysis indeterminate.[30] Notably, in 2015 ethylene has been selectively converted to butadiene over FAU-supported $Rh(CO)_2$ and $Rh(CO)(C_2H_4)$ single-atom catalysts at 25 °C and 1 atm under continuous ethylene flow, yielding a TOF of ~2 h^{-1},[17] marking the discovery of the dehydrogenative coupling of ethylene into butadiene ($2C_2H_4 \rightarrow C_4H_6 + H_2$). In 2018, an $Ir(C_2H_4)_2$(Phebox) organometallic complex was shown to convert ethylene catalytically *via* $3C_2H_4 \rightarrow C_4H_6 + C_2H_6$ with butene by-products [$S_{C_4H_6} < 45\%$; P: 2–12 atm; TOF: 0.25 h^{-1} at 2 atm/100 °C, 0.9 h^{-1} at 12 atm/110 °C].[31] Despite this progress, the catalytic chemistry of butadiene formation from a cheap ethylene feedstock under mild conditions remains unattained, demonstrating the relevance of the observed butadiene activity at 120 °C for Ni/BEA. We note that fast deactivation at this temperature is not surprising considering that H-zeolites are often used as butadiene adsorbents.[32]

After catalysis, exposure of the sample to CO restores the original 2211 cm^{-1} feature (Fig. S16 and S17†), but to a lesser extent due to unsaturated carbonaceous deposits blocking the active sites, further confirmed by *in situ* ^{13}C NMR (Fig. S24†).[33] The absence of vibrational signatures for Ni(I) and Ni(0) carbonyl complexes further suggests that no reduction of Ni(II) occurred during ethylene dimerization and that Ni(II) in the ion-exchange positions of the zeolite is the active site in ethylene dimerization (Fig. S17†).

Moreover, post-reaction (200 °C in ethylene flow) CO adsorption reveals a peak around ~2230 cm^{-1} (Fig. S16 and 17†) not present in the fresh sample. This corresponds to CO adsorbed on extraframework aluminium[34] formed under mild catalytic conditions in the presence of Ni(II) atoms and ethylene. Solid-state NMR further confirms this result *via* comparison of ^{27}Al MAS NMR spectra of fresh and spent samples (Fig. S19†) which show that dealumination indeed occurs under mild conditions, evidenced by a feature at ~30 ppm due to the presence of penta-coordinate extraframework Al sites as well as broadening of tetrahedral Al bands. Such mild conditions have been not previously reported to cause dealumination of the zeolite framework. This is likely due to polymerization of ethylene in the microporous channels and the subsequent breakage of pores.

In addition to the supported d^8 Ni(II) species, a 0.7 wt% $Ir(CO)_2$ species was prepared on H-FAU zeolite with Si/Al ~ 15 as for Ni/BEA. This formulation was previously characterized with EXAFS and FTIR,[35] where its interaction with ethylene was reported to produce $Ir(CO)(C_2H_4)$ complexes. Pulses of ethylene, followed by inert gas purging indeed produce only the $Ir(CO)(C_2H_4)$ complex in this study (Fig. 2A and C).

DRIFTS confirms the successful grafting of the complex with the formation of symmetric and asymmetric CO stretches of the square-planar $Ir(CO)_2$ fragment at 2108 and 2038 cm^{-1}.[12,17,18] HAADF-STEM imaging (Fig. S20† and 2B) further confirms site-isolated nature of the complex in the zeolite micropores. Sample exposure to flowing pure C_2H_4 in the DRIFTS cell revealed transient behavior (Fig. 3).

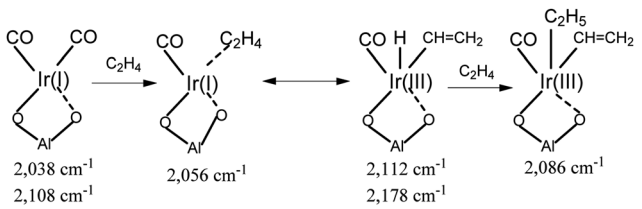

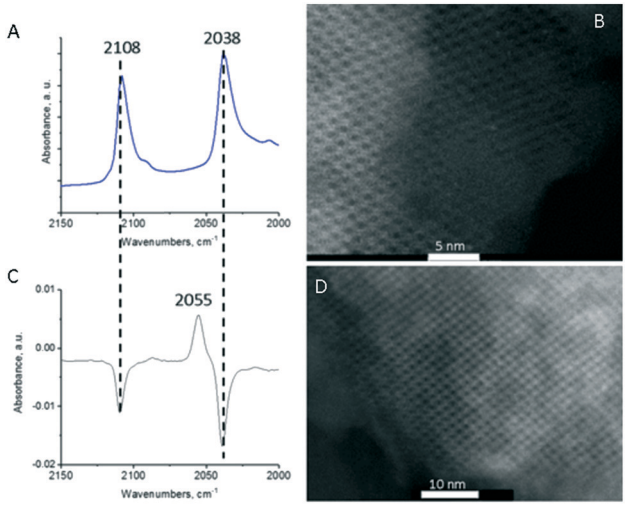

Fig. 2 A). DRIFTS spectrum of the starting 0.7% $Ir(CO)_2$/FAU Si/Al ~ 15 material B). High-resolution HAADF-STEM image of the fresh Ir/FAU in [110] projection, individual Ir atoms can be seen in the supercages C). DRIFTS difference spectrum during reaction of $Ir(CO)_2$/FAU with pulses of dilute ethylene, showing disappearance of 2108 and 2038 cm^{-1} bands of $Ir(CO)_2$ and appearance of only 1 new band at 2055 cm^{-1}, belonging to $Ir(CO)(C_2H_4)$/FAU complex. D). High-resolution HAADF-STEM image of $Ir(CO)_2$/FAU after ethylene catalysis at 225 °C for 1 hour, in the [110] projection, showing lack of Ir agglomeration.

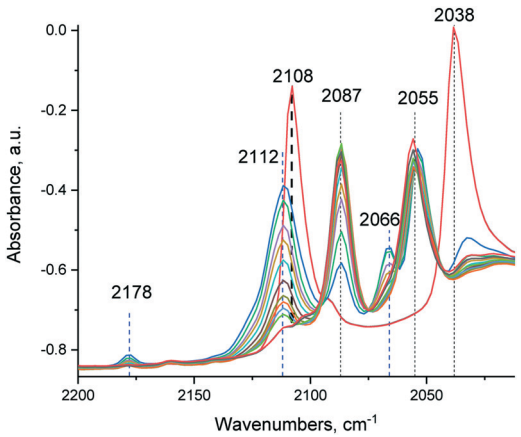

Fig. 3 DRIFTS spectrum of 0.7% $Ir(CO)_2$/FAU Si/Al ~ 15 during exposure to flowing pure ethylene (the first 5 minutes).

The peaks, belonging to the symmetric and asymmetric CO stretches of $Ir(CO)_2$, at 2108 and 2038 cm^{-1} declined while new features emerged. The 2055 cm^{-1} feature has been previously assigned to the $Ir(CO)(C_2H_4)$ complex;[12,17,18] however, careful inspection of the spectra in the 2060–2030 cm^{-1} region reveals new features (Fig. 4): the 2066 and 2053 cm^{-1} peaks decrease in concert as the 2056 cm^{-1} feature of $Ir(CO)(C_2H_4)$ grows with clear isosbestic points (shaded).

This indicates the stoichiometric transformation of $Ir(CO)_2$ into $Ir(CO)(C_2H_4)$, occurring *via* the following sequence:

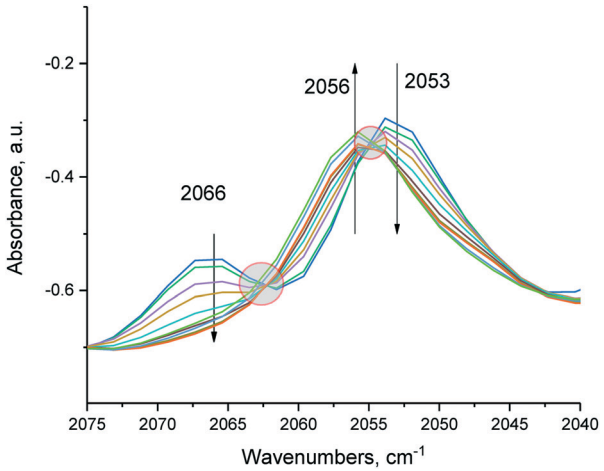

Fig. 4 DRIFTS spectrum of 0.7% $Ir(CO)_2$/FAU Si/Al ~ 15 during exposure to flowing ethylene (initial 5 minutes).

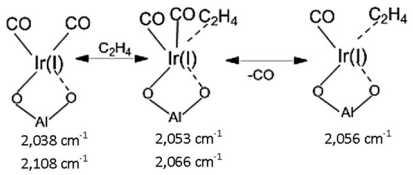

Initially, the square-planar $Ir(CO)_2$ accepts one C_2H_4 ligand to form a $Ir(CO)_2(C_2H_4)$ species which then expels one CO ligand, forming square-planar $Ir(CO)(C_2H_4)$. Concomitantly bands at 2178 cm^{-1} (weak) and 2112 cm^{-1} (intense) develop within the first 1 minute of ethylene exposure (Fig. 5).

The intense 2112 cm^{-1} band belongs to the CO vibration of an oxidized Ir center (CO adsorbed on metal cations has high molar extinction coefficients) and the low intensity 2178 cm^{-1} band corresponds to the Ir–H stretching vibration. Indeed, this fully agrees with the described synthesis of the first supported, transition metal carbonyl hydride complexes of Rh(III)$(H)_x(CO)$ and relatively low intensity of Rh–H stretching vibrations compared to CO vibrations.[17,18] We note

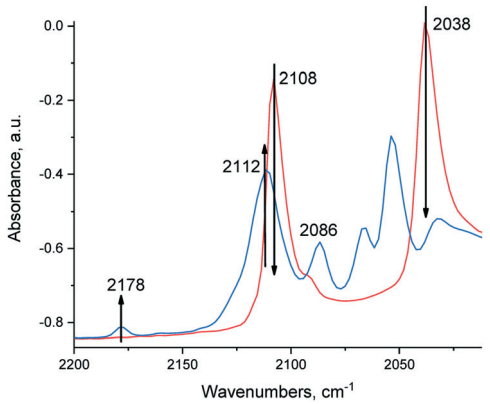

Fig. 5 DRIFTS spectrum of 0.7% $Ir(CO)_2$/FAU Si/Al ~ 15 during exposure to ethylene (~1 minute). 2178 and 2112 cm^{-1} grow in concert.

that Rh(III) and Ir(III) have the same d^6 electronic configuration and provide the analogous (to Rh) synthesis of Ir(III) carbonyl hydride complex,[18] unambiguously identifying the Ir–H stretch at 2150 cm^{-1}. Analogous to the selective synthesis of $Rh(III)(CO)H_2$ complexes from $Rh(CO)_2$,[18] the $Ir(CO)H_x$ species has been suggested from treatments of $Ir(CO)_2$/FAU with ethylene followed by hydrogen.[35] In that study, the authors failed to identify the Ir–H stretch, concluding that its signature is too weak to be observed. We treated our $Ir(CO)_2$ materials with C_2D_4, forming first $Ir(I)(CO)(C_2D_4)$ which we then exposed to H_2 flow (Fig. S29–S31†). Both the actual spectra and difference spectra indicate selective conversion of $Ir(CO)(C_2D_4)$ to the $Ir(CO)(H)_2$ complex with CO stretching observed at 2065 cm^{-1} and the Ir–H stretch at 2150 cm^{-1}. Isotopic shift experiments with D_2 (Fig. S31†) confirm that the 2150 cm^{-1} is indeed the Ir–H stretch.

As such, the simultaneous formation of new Ir–H and Ir–CO stretches (Fig. 5 and 6) arises from the generation of one species. The high-lying stretch of Ir–CO means that Ir is in the +3 oxidation state, signifying the unprecedented oxidative addition of the C–H bonds of ethylene to the Ir(CO) fragment with the formation of $Ir(III)(CO)(H)(C_2H_3)$ carbonyl vynil hydrido-complex: C_2H_4–Ir(I)–CO ↔ C_2H_3–Ir(III)(H)(CO). These assignments and described behavior are further supported by observation of these species the *in situ* NMR data (Fig. S23†).

As the concentration of this complex reaches its maximum (~1 minute), the intensities of both the 2112 and 2178 cm^{-1} features reach their maxima and then decline in concert as a new CO stretching band develops at 2086 cm^{-1} that has no corresponding Ir–H stretching band (Fig. 6). This indicates the hydride is consumed during the reaction with ethylene. This suggests the consequent formation of an $Ir(III)(CO)(C_2H_5)(C_2H_3)$ complex *via* ethylene insertion into the Ir–H bond.

Furthermore, in order to unambiguously assign the 2178 cm^{-1} band to the Ir–H stretch, we replicated the infrared experiment on $Ir(CO)_2$ and C_2H_4 with C_2D_4. We observed the absence of the 2178 cm^{-1} band (Ir–H stretch), upon oxidative addition of C_2D_4 to the Ir(I) center. Instead, Ir(III)–D species forms (Fig. S32†).

The observed room-temperature activation of C–H bonds with the formation of iridium carbonyl alkyl hydride complex is unprecedented. Such transformation have been only rarely described in organometallic literature[36] and never directly observed spectroscopically on any solid material. The bond is not split heterolytically on the M–O bond but instead it is activated homolytically *via* oxidative addition to an electrophilic d^8 metal center in the zeolite micropore. High coordinative unsaturation and superelectrophilicity of M cations in zeolite have been recently quantified for isoelectronic d^8 Pd(II) ions,[23] explaining why this reaction is favored over heterolytic activation of C–H bonds on covalent M–O bond. It is important to note that such a homolytic pathway of C–H bond activation has been previously overlooked in the metal/zeolite and M/oxide literature. Indeed, heterolytic activation of strong X–H bonds (C–H of

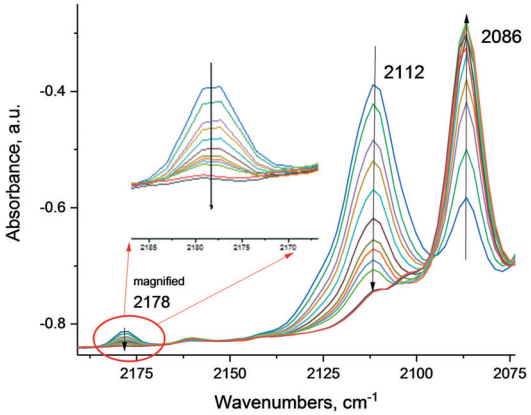

Fig. 6 DRIFTS spectrum of 0.7% $Ir(CO)_2$/FAU during exposure to ethylene (~5 minutes). The 2112 and 2178 cm^{-1} bands decline simultaneously as the 2087 cm^{-1} feature grows.

hydrocarbons and N–H of ammonia) normally require relatively high temperatures.[37,38]

Ethylene activity over $Ir(CO)_2$/FAU produces measurable amounts of butenes at temperatures above 80 °C and butadiene at temperatures above 180 °C with the maximum rate of catalytic butadiene production at ~200–220 °C and selectivities to butadiene on the order 17–20% (Table S2†). After catalysis, Ir remains site-isolated and does not agglomerate into Ir nanoparticles as evidenced by HAADF-STEM and FTIR data (Fig. 2D and S21 and S22†). Formation of carbonaceous polymeric deposits, framework breakage, and dealumination similar to Ni/BEA is also observed (Fig. S20, S21 and S25†). The ease with which oxidative addition of ethylene C–H bond to highly electrophilic Ir(I) center takes place at room temperature at 1 bar pressure of ethylene, suggests that C–H activation is not the rate-limiting step of the ethylene dimerization under these conditions: C–C coupling and/or beta-hydride elimination are expected to be rate-limiting steps in catalysis.

We construct two plausible catalytic pathways for butadiene (and butene) production. Two different steps of initial C–H bond activation are possible: 1) homolytic activation of C–H bond *via* oxidative addition to M d^8 center, which we observe experimentally (Fig. S26†) and 2) heterolytic activation of C–H bond on the M-ozeolite pair (Fig. S27†), which we did not observe. Two ethylene molecules could also couple on single d^8 metal center with the formation of metallacyclopentane species (Fig. S28†), that were shown by Goldman and co-workers to form on $Ir(C_2H_4)_2$(Phebox) system by trapping *via* CO.[31] The stability of the species, as noted previously by Halpern,[39] does not mean that it is the true active state of the catalyst. Indeed, most active species are formed transiently (as we observe experimentally for $Ir(III)(H)(CO)(C_2H_3)$ species), hence mechanism in Fig. S26† is most likely operative.

Furthermore, deeper mechanistic insight into the pathway of butadiene production was achieved by refuting the direct dehydrogenation of butene into butadiene. When 1-butene

was introduced to the catalyst at 150–200 °C, no butadiene was observed. Thus, the route to butadiene mechanistically differs from direct butene dehydrogenation. Indeed, such dehydrogenation does not take place on single Ir atoms under such mild conditions.

Notably, in the most probable reaction mechanism depicted in Fig. S26,† we propose 1-butene formation directly from Ir(III)(CO)(C_2H_5)(C_2H_3) and Ni(IV)(C_2H_5)(C_2H_3) *via* reductive elimination of the ethyl and vinyl fragments with restoration of Ni(II) and Ir(I)–CO fragments which reform Ni(II)(C_2H_4) and Ir(I)(CO)(C_2H_4) in the presence of ethylene. It is also possible that beta-hydride elimination releases 1-butene from the M-(*n*-butyl) intermediate, which forms when the ethyl group in M(C_2H_4)(C_2H_5) migrates. Butadiene may be formed analogous to this scheme but in this case the vinyl group of M(C_2H_3)(C_2H_4) fragment migrates, forming M–CH_2–CH_2–CH=CH_2, from which *via* beta-hydride elimination butadiene-1,3 is released.

These findings for supported Ni(II) and Ir(I) isolated sites may help reveal mechanistic uncertainties for the Cr/SiO_2 Phillips ethylene polymerization catalyst, extensively studied over 50 years. Though believed to follow a Cossee–Arlman Cr-alkyl mechanism, the low number of active sites (<10%), amorphous silica support, fast reaction rates, and the presence of multiple oxidation states of Cr prevented a thorough understanding of the initiation mechanism. Recent elegant studies[40] demonstrated that Cr(II) sites are required to start ethylene polymerization, and earlier kinetic studies suggested schemes consistent with activation of ethylene on Cr(II) sites to form Cr(IV) vinyl hydride,[41,42] though this species has never been observed. Based on our current findings, we suggest that the active fraction of the catalyst could be the highly electrophilic Cr(II) species that can add ethylene *via* C–H oxidative addition to form a Cr(IV)-vinyl (C_2H_3)-hydride (H) species:

$$Cr(II) + C_2H_4 \leftrightarrow Cr(IV)(H)(CH{=}CH_2)$$

The formation of Cr-ethyl follows:

$$Cr(IV)(H)(CH{=}CH_2) + C_2H_4 \rightarrow Cr(IV)(C_2H_4)(H)(C_2H_3) \rightarrow Cr(IV)(C_2H_5)(C_2H_3).$$

Cr(IV)(C_2H_5)(C_2H_3) sites may facilitate longer alkyl chain formation *via* alkyl migration:

$$Cr(C_2H_5)(C_2H_3) + C_2H_4 \rightarrow Cr(C_2H_4)(C_2H_5)(C_2H_3) \rightarrow Cr(C_4H_9)(C_2H_3)$$

$$Cr(IV)(C_4H_9)(C_2H_3) + nC_2H_4 \rightarrow Cr(IV)[(CH_2)_{3+2n}CH_3](C_2H_3)$$

Subsequently, direct reductive elimination of $CH_3(CH_2)_x$-CH=CH_2 is possible which restores the Cr(II) site and re-starts the catalytic cycle:

$$Cr(IV)[(CH_2)_x{-}CH_3](C_2H_3) \rightarrow Cr(II)/SiO_2 + CH_3{-}(CH_2)_x{-}CH{=}CH_2$$

Beta-hydride elimination from Cr(IV)[$(CH_2)_x$–CH_3](C_2H_3) could also restore Cr(IV)(H)(C_2H_3) and re-start the polymerization cycle:

$$Cr(IV)[(CH_2)_x{-}CH_3](C_2H_3) \rightarrow Cr(IV)(H)(C_2H_3) + CH_3{-}(CH_2)_{x-2}{-}CH{=}CH_2$$

The proposed mechanism does not contradict experimental observations and provides a plausible explanation for the initiation uncertainties of the Phillips catalyst. Furthermore, support for this proposed mechanism is obtained from recent works, in which –CH_2–CH_2–CH=CH_2 sites were suggested to form on the catalyst.[43] These sites can form from the vinyl migration in the following reaction sequence:

$$Cr(IV)(C_2H_5)(C_2H_3) + C_2H_4 \rightarrow Cr(IV)(C_2H_4)(C_2H_5)(CH{=}CH_2) \rightarrow Cr(IV)(C_2H_5)(CH_2{-}CH_2{-}CH{=}CH_2)$$

In conclusion, we provide the first experimental mechanistic evidence of how ethylene dimerization occurs and proceeds on d^8 M(I and II) cations in zeolites in the absence of an initial M–H species: the M–H bond is formed *via* the homolytic activation of ethylene's C–H bond (stronger than that of methane) on very electrophilic Ir(I) sites in the zeolite micropore. Further, the preparation of well-defined Ir(I) and Ni(II) d^8 in zeolites is demonstrated and accompanied by new chemistry and characterization for both systems before and after catalysis. Both Ni(II) and Ir(I) in zeolites produce butenes and, unprecedentedly, butadiene upon reaction with ethylene under mild conditions. Notably, Ni is more active at lower temperatures toward C–H bond activation than the expensive Ir.

Conflicts of interest

The authors declare no competing financial interests.

Acknowledgements

The research described in paper is part of the Quickstarter Initiative at Pacific Northwest National Laboratory. It was conducted under the Laboratory Directed Research and Development Program at PNNL, a multiprogram national laboratory operated by Battelle for the U.S. Department of Energy (DOE) under Contract DE-AC05-76RL01830. The research described in this paper was performed in the Environmental Molecular Sciences Laboratory (EMSL), a national scientific user facility sponsored by the DOE's Office of Biological and Environmental Research. This work was supported by US Department of Energy, Office of Science, Office of Basic Energy Sciences, Division of Chemical Sciences, Biosciences, and Geosciences.

References

1 W. M. H. Sachtler, *Catal. Today*, 1992, **15**(3–4), 419–429.
2 K. Klier, *Langmuir*, 1988, **4**(1), 13–25.
3 F. Lonyi, A. Kovacs, A. Szegedi and J. Valyon, *J. Phys. Chem. C*, 2009, **113**(24), 10527–10540.

4 A. Corma and H. Garcia, *Top. Catal.*, 2008, **48**(1–4), 8–31.
5 A. Haruta, *Chem. Rec.*, 2003, **3**(2), 75–87.
6 R. Barrer, *Surface Organometallic Chemistry: Molecular Approaches to Surface Catalysis*, in Zeolite Synthesis: An Overview, ed. J.-M. Basset, B. C. Gates, J.-P. Candy, A. Choplin, M. Leconte, F. Quignard and C. Santini, Kluwer Academic Publishers, 1988, pp. 221–244.
7 J. H. Kwak, D. Tran, S. D. Burton, J. Szanyi, J. H. Lee and C. H. F. Peden, *J. Catal.*, 2012, **289**, 272.
8 W. M. H. Sachtler, *Acc. Chem. Res.*, 1993, **26**(7), 383–387.
9 K. Khivantsev, N. R. Jaegers, L. Kovarik, J. C. Hanson, F. Tao, Y. Tang, X. Y. Zhang, I. Z. Koleva, H. A. Aleksandrov, G. N. Vayssilov, Y. Wang, F. Gao and J. Szanyi, *Angew. Chem., Int. Ed.*, 2018, **57**(51), 16672–16677.
10 A. Finiels, F. Fajula and V. Hulea, *Catal. Sci. Technol.*, 2014, **4**(8), 2412–2426.
11 J. Baiale, *US Pat.*, US3738977A, 1971.
12 K. Khivantsev, A. Vityuk, H. A. Aleksandrov, G. N. Vayssilov, D. Blom, O. S. Alexeev and M. D. Amiridis, *ACS Catal.*, 2017, **7**(9), 5965–5982.
13 I. Agirrezabal-Telleria and E. Iglesia, *J. Catal.*, 2017, **352**, 505–514.
14 A. C. Yang and C. W. Garland, *J. Phys. Chem.*, 1957, **61**(11), 1504–1512.
15 H. Knozinger, E. W. Thornton and M. Wolf, *J. Chem. Soc., Faraday Trans. 1*, 1979, **75**, 1888–1899.
16 P. Serna and B. C. Gates, *Angew. Chem., Int. Ed.*, 2011, **50**(24), 5528–5531.
17 K. Khivantsev, *PhD Thesis*, University of South Carolina, 2015.
18 K. Khivantsev, A. Vityuk, H. A. Aleksandrov, G. N. Vayssilov, O. S. Alexeev and M. D. Amiridis, *J. Phys. Chem. C*, 2015, **119**(30), 17166–17181.
19 R. Joshi, G. H. Zhang, J. T. Miller and R. Gounder, *ACS Catal.*, 2018, **8**(12), 11407–11422.
20 R. Y. Brogaard and U. Olsbye, *ACS Catal.*, 2016, **6**(2), 1205–1214.
21 N. R. Jaegers, J. K. Lai, Y. He, E. Walter, D. A. Dixon, M. Vasiliu, Y. Chen, C. M. Wang, M. Y. Hu, K. T. Mueller, I. E. Wachs, Y. Wang and J. Z. Hu, *Angew. Chem., Int. Ed.*, 2019, **131**, 12739–12746.
22 S. Moussa, P. Concepcion, M. A. Arribas and A. Martinez, *ACS Catal.*, 2018, **8**(5), 3903–3912.
23 K. Khivantsev, N. R. Jaegers, I. Z. Koleva, H. A. Aleksandrov, L. Kovarik and M. Engelhard, *et al.*, Stabilization of Super Electrophilic Pd+2 Cations in Small-Pore SSZ-13 Zeolite, *ChemRxiv*, 2019, 1–49, Preprint, DOI: 10.26434/chemrxiv.7789454.v2.
24 K. Khivantsev, N. R. Jaegers, L. Kovarik, S. Prodinger, M. A. Derewinski, Y. Wang, F. Gao and J. Szanyi, *Appl. Catal., A*, 2019, **569**, 141–148.
25 K. Khivantsev, F. Gao, L. Kovarik, Y. Wang and J. Szanyi, *J. Phys. Chem. C*, 2018, **122**(20), 10820–10827.
26 P. S. Petkov, H. A. Aleksandrov, V. Valtchev and G. N. Vayssilov, *Chem. Mater.*, 2012, **24**(13), 2509–2518.
27 G. Pomalaza, M. Capron, V. Ordomsky and F. Dumeignil, *Catalysts*, 2016, **6**(12), 203–237.
28 V. L. Dagle, M. D. Flake, T. L. Lemmon, J. S. Lopez, L. Kovarik and R. A. Dagle, *Appl. Catal., B*, 2018, **236**, 576–587.
29 V. L. Sushkevich and I. I. Ivanova, *Appl. Catal., B*, 2017, **215**, 36–49.
30 S. A. Cohen, P. R. Auburn and J. E. Bercaw, *J. Am. Chem. Soc.*, 1983, **105**(5), 1136–1143.
31 Y. Gao, T. J. Emge, K. Krogh-Jespersen and A. S. Goldman, *J. Am. Chem. Soc.*, 2018, **140**(6), 2260–2264.
32 A. M. Tsybulevski, L. M. Kustov, K. C. Weston, A. A. Greish, O. P. Tkachenko and A. V. Kucherov, *Ind. Eng. Chem. Res.*, 2012, **51**(20), 7073–7080.
33 N. R. Jaegers, M. Y. Hu, D. W. Hoyt, Y. Wang and J. Z. Hu, Development and Application of In Situ High-Temperature, High-Pressure Magic Angle Spinning NMR, in *Modern Magnetic Resonance*, ed. G. A. Webb, Springer International Publishing, Cham, 2017, pp. 1–19.
34 J. Szanyi and M. T. Paffett, *Microporous Mater.*, 1996, **7**(4), 201–218.
35 C. Martinez-Macias, P. Serna and B. C. Gates, *ACS Catal.*, 2015, **5**(10), 5647–5656.
36 D. M. Haddleton and R. N. Perutz, *J. Chem. Soc., Chem. Commun.*, 1986, 1734–1736.
37 K. Khivantsev, A. Biancardi, M. Fathizadeh, F. Almalki, J. L. Grant, H. N. Tien, A. Shakouri, D. A. Blom, T. M. Makris, J. R. Regalbuto, M. Caricato and M. Yu, *ChemCatChem*, 2018, **10**(4), 736–742.
38 B. Hu, A. Getsoian, N. M. Schweitzer, U. Das, H. Kim, J. Niklas, O. Poluektov, L. A. Curtiss, P. C. Stair, J. T. Miller and A. S. Hock, *J. Catal.*, 2015, **322**, 24–37.
39 A. S. Goldman, C. R. Landis and A. Sen, *Angew. Chem., Int. Ed.*, 2018, **57**(17), 4460–4460.
40 E. Morra, G. A. Martino, A. Piovano, C. Barzan, E. Groppo and M. Chiesa, *J. Phys. Chem. C*, 2018, **122**(37), 21531–21536.
41 Y. V. Kissin and A. J. Brandolini, *J. Polym. Sci., Part A: Polym. Chem.*, 2008, **46**(16), 5330–5347.
42 P. Zielinski and I. G. D. Lana, *J. Catal.*, 1992, **137**(2), 368–376.
43 A. Chakrabarti, M. Gierada, J. Handzlik and I. E. Wachs, *Top. Catal.*, 2016, **59**(8–9), 725–739.

